

# A Solid-State Rearrangement During Solvothermal MOF Synthesis Observed by *In Situ* Diffraction

Yue Wu,<sup>‡</sup> Saul J. Moorhouse,<sup>‡</sup> Matthew J. Cliffe and Dermot O'Hare\*

Department of Chemistry, University of Oxford, Oxford, OX1 3TA, U.K.

---

**ABSTRACT:** Time-resolved, *in situ* high energy angular dispersive X-ray powder diffraction (ADXRD) of the hydrothermal synthesis of  $(\text{H}_2\text{NMe}_2)_2[\text{Co}_3(\text{BDC})_4]\cdot y\text{DMF}$  proceeds via a topotactic rearrangement in which a structurally-related metastable precursor evolves into the final product via the inter-layer reordering.

---

## Introduction

In MOF synthesis, a number of distinct frameworks can often be produced from the same mixture of reagents under the same conditions, suggesting that the energy landscape is relatively flat. Many of these phases might be considered metastable with regard to the most stable MOF formed in a reaction system. In exploratory MOF synthesis, the accepted method is to combine the reagents and solvent in a solvothermal reactor and heat at 80–200 °C for 1–2 days, then isolate any crystalline products. Due to the relatively long reaction times and high temperatures, this method has been proven to be a convenient and effective method of furnishing the most thermodynamically stable MOF from a given mixture.

One drawback with this approach is that it is difficult in to study the formation of MOFs *in situ*, as the necessity for reaction vessels to be heat- and pressure-resistant also makes them more resistant to experimental probes such as X-rays. As a result, understanding of MOF formation lags behind research on chemical and structural properties. The existing literature on *in situ* diffraction studies of MOF formation remains sparse. The most common technique used has been energy dispersive X-ray diffraction (EDXRD);<sup>1–8</sup> more recently, advances in technology have made monochromatic or angular dispersive XRD (ADXRD) experiments feasible.<sup>9</sup> Techniques such as SAXS-WAXS,<sup>10</sup> XANES<sup>11</sup> and liquid cell TEM<sup>12</sup> have also been used for *in situ* studies, but more specialized sample environments are generally required. In this paper, we present research performed on our recently constructed Oxford-Diamond *In Situ* Cell (ODISC) furnace, designed for beamline I12 at the Diamond Light Source (UK).<sup>13</sup> This setup enables for the first time the *in situ* study of laboratory-scale solvothermal reactions (*ca.* 5 – 20 mL) using high X-ray energy (53.2 keV) ADXRD. An advantage of the larger-scale sample environment is that we are able to study more conventional laboratory reaction setups using high resolution XRD: herein, we report a MOF synthesis that uses cation-exchanged polymer resin beads as both

template and metal source - a relatively new technique in MOF synthesis that can enable access to new phases.<sup>14–16</sup>

In many cases, a given combination of metal ion and ligand can give rise to several different possible MOFs. Within a reaction, a metastable phase will often form first as an intermediate. In some cases, there is evidence that the preorganization of the reagents in the intermediate is partially retained in the transformation to the final phase. Examples include the aluminium –  $\text{NH}_2$ -BDC (BDC = 1,4-benzenedicarboxylate) system, in which various routes to MIL-53(Al) were observed, including a  $\text{MOF-235} \rightarrow \text{MIL-101} \rightarrow \text{MIL-53}$  pathway.<sup>10</sup> A  $\text{MOF-235} \rightarrow \text{MIL-53}$  pathway was also observed in the formation of MIL-53(Fe).<sup>2</sup> Framework isomers arising from the same reaction system have also been observed in *ex situ* experiments, for example in the V(III)-bdc system, in which it is shown both MIL-101(V) and MIL-88B(V) will convert to MIL-47 under certain conditions, while MIL-47 can also be formed as a pure phase. In the pillared paddlewheel M(II)-bdc-dabco frameworks, the square-grid topologies can be accessed through a kagome topology with identical chemical connectivity.<sup>17</sup>

In the cases discussed above, the intermediate/precursor phases generally undergo a dissolution-recrystallization process to form a more thermodynamically stable phase. In this paper, we report the first direct observation of a rapid topochemical solid-state rearrangement of crystalline intermediate to product during the formation of a MOF. We studied the Co-BDC-DMF (DMF = N,N-dimethylformamide) system, from which a large number of structurally related monoclinic phases can arise, all constructed from linear trinuclear cobalt-carboxylate clusters interconnected by BDC ligands and having the general formula  $(\text{H}_2\text{NMe}_2)_2[\text{Co}_3(\text{BDC})_4]\cdot y\text{DMF}$  ( $y$  = variable amount of uncoordinated solvent). The  $\text{Co}_3$  clusters tend to form highly connected sheets in which they lie parallel to each other; the sheets are then pillared by additional BDC moieties (Figure 1a). The structural variability arises from the possibility of different coordination modes of the  $\text{Co}_3$  clusters. The central cobalt in

each cluster always has octahedral coordination ( $\text{Co}_{\text{oct}}$ ), while the terminal cobalt atom can exist in distorted octahedral, tetrahedral ( $\text{Co}_{\text{tet}}$ ) or pyramidal ( $\text{Co}_{\text{pyr}}$ ) environments with either single ( $\text{Co}_{\text{tet}}$ ) or double ( $\text{Co}_{\text{oct}}$  and  $\text{Co}_{\text{pyr}}$ ) coordination at the terminal carboxylate; all known clusters have symmetric terminal coordinations.<sup>18</sup> Charge balance is provided by the dimethylammonium decomposition products of the DMF solvent. Every known structure contains symmetric  $\text{Co}_3$  clusters and takes the  $\text{C}_2/c$  symmetry, with the main difference being the shear angle between the layers corresponding to the monoclinic  $\beta$  angle. This demonstrates that the energy landscape for Co-BDC polymorphs is very flat, suggesting the possibility of phase interconversion during synthesis. Moreover, it is clear that in many cases, these interconversions can take place while conserving the layer structure (Figure 1b).

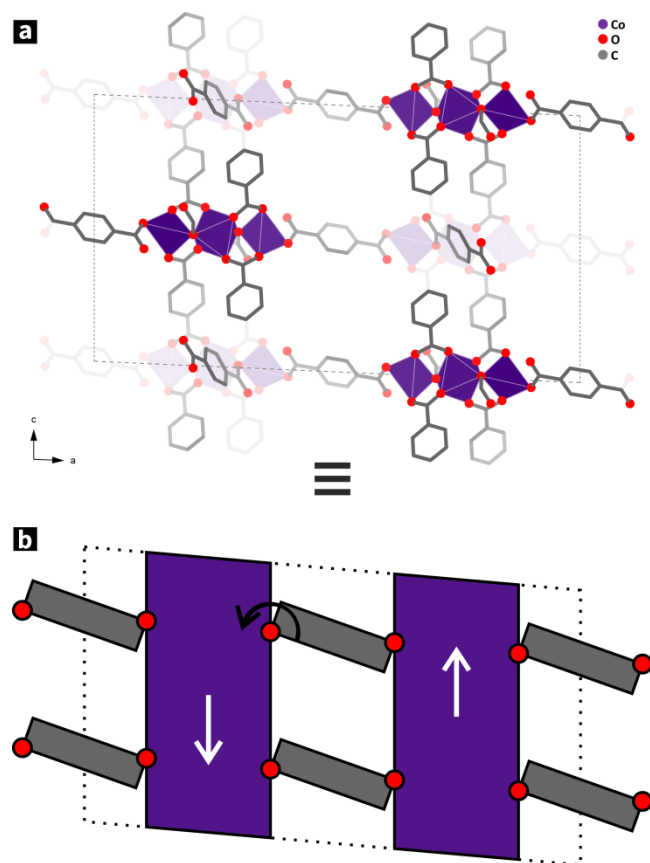


Figure 1. (a) The  $(\text{H}_2\text{NMe}_2)_2[\text{Co}_3(\text{BDC})_4]\cdot y\text{DMF}$  framework viewed along the  $b$ -axis. The trinuclear ccooordination cluster contains one octahedral Co and two tetrahedral Co atoms. For clarity, hydrogen and non-framework atoms from  $\text{H}_2\text{NMe}_2^+$  and DMF are omitted. Octahedral and tetrahedral Co coordination spheres are drawn as polyhedra. (b) Schematic representation of the framework structure of  $(\text{H}_2\text{NMe}_2)_2[\text{Co}_3(\text{BDC})_4]\cdot y\text{DMF}$  showing the possibility of low-energy interlayer shearing.

## Results and discussion

Figure 2a shows a contour plot of the time-resolved *in situ* ADXRD data for the reaction of Co(II)-exchanged resin beads and BDC in DMF at 250 °C. The initial region ( $t < 10$  min) corresponds to the heating of the reactor and the dissolution of BDC (full details in ESI). The second region ( $10 \text{ min} < t < 20 \text{ min}$ ) corresponds to the crystallization of a transient intermediate phase. At  $t > 20$  min, this intermediate disappears with the concomitant formation of a phase-pure crystalline product. The ADXRD of the final product can be refined to a known Co-BDC phase. The lack of sufficient non-overlapping Bragg reflections and the low crystal symmetry have meant that we are unable to fully index the intermediate phase (see ESI). However, sequential peak fitting of the observed the Bragg reflections have allowed several important conclusions to be drawn.

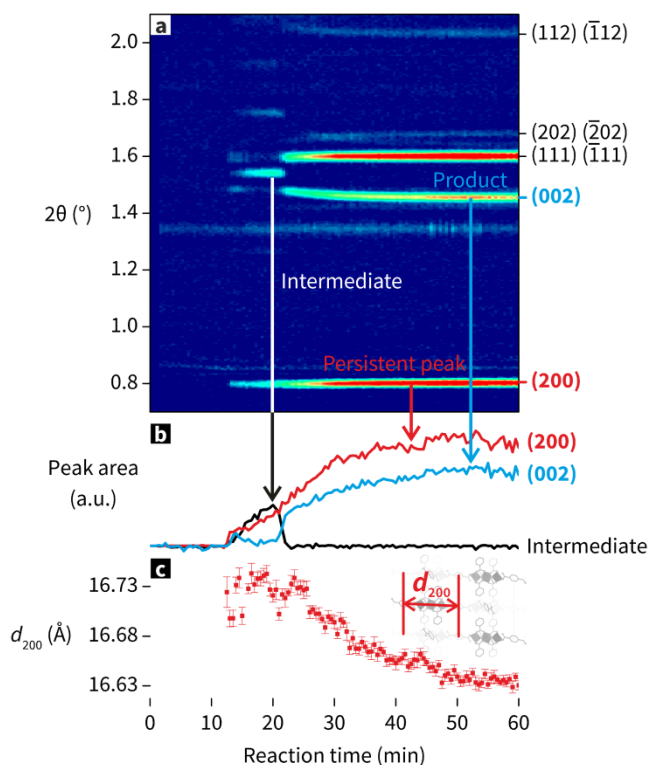


Figure 2. Time-resolved, high energy *in situ* angular-dispersive XRD data from the hydrothermal synthesis of  $(\text{H}_2\text{NMe}_2)_2[\text{Co}_3(\text{BDC})_4]\cdot y\text{DMF}$  at 250 °C. a) Contour plot of background-subtracted data with reflections from the product phase labelled. b) Time dependence of the peak areas of the 200 and 002 Bragg reflection of  $(\text{H}_2\text{NMe}_2)_2[\text{Co}_3(\text{BDC})_4]\cdot y\text{DMF}$ , and the most intense non-overlapping Bragg reflection of intermediate phase. c) Time dependence of interlayer  $d$ -spacing in  $(\text{H}_2\text{NMe}_2)_2[\text{Co}_3(\text{BDC})_4]\cdot y\text{DMF}$  calculated from the position of the 200 Bragg reflection.

Figure 2 shows that the 200 Bragg reflection of  $(\text{H}_2\text{NMe}_2)_2[\text{Co}_3(\text{BDC})_4]\cdot y\text{DMF}$  co-exists during the formation of the crystalline intermediate phase, indicating that these two materials are structural related. Peak fit-

ting of the 200 Bragg reflection shows that its intensity grows smoothly throughout the reaction. The growth profile of the 200 Bragg reflection intensity is typical for a hydrothermal reaction of this type. The  $t_{1/2}$  is ca. 30 min, the data can be fitted the [??? equation](#). Surprisingly, we do not see any narrowing of the peak width at half maximum (PWHM) during  $(\text{H}_2\text{NMe}_2)_2[\text{Co}_3(\text{BDC})_4]\cdot y\text{DMF}$  crystallization which may be due domination from instrumental line broadening terms.

Interestingly, the most intense Bragg reflection assigned to the intermediate phase has the same temporal dependence over the first 20 min, at which point it abruptly disappears in ca. 2 min, with a correspondingly abrupt increase in the intensity of the Bragg reflections due to the final product (Figure 2b). This transition is unusually rapid, much faster than would be expected for any type of dissolution-recrystallization type behaviour. The 200 Bragg reflection corresponds to the interlayer spacing between the sheets in the framework, implying that the intermediate and product frameworks are structurally related with a very similar interlayer distance. The change in the (200) peak position (Figure 2c) shows that the interlayer distance decreases by ca. 0.1 Å from intermediate to product. A likely explanation for this is interlayer shearing from intermediate to product: if only the  $\beta$  angle of the monoclinic cell is changed, a 0.1 Å change in interlayer distance equates to a ca. 6° change in  $\beta$ , which also corresponds to the interlayer shear angle. The energy of this mechanism would be particularly low if the layers were pillared by BDCs with singly coordinated carboxylates (Figure 1b). The *in situ* ADXRD of the product phase is of sufficient quality to enable Rietveld refinement, the best fit corresponds most closely to a structure in which the carboxylate of the pillaring BDC is singly coordinated to a tetrahedral Co, reported by Wang and co-workers as phase 2.<sup>18</sup> [\[ESI: single in-situ pattern refinements\]](#)

The low energy difference between different phases is demonstrated directly and systematically by a comparison of the products from the same experimental setup over a range of temperatures (180, 200, 225 and 250 °C). While *in situ* data from the syntheses at the three lower temperatures were too weak to extract useful mechanistic information, refinement of PXRD patterns of the collected products provided additional information (full refinements are included in ESI). The data were collected post synthesis on product suspended in mother liquor, in order to mimic reaction conditions.

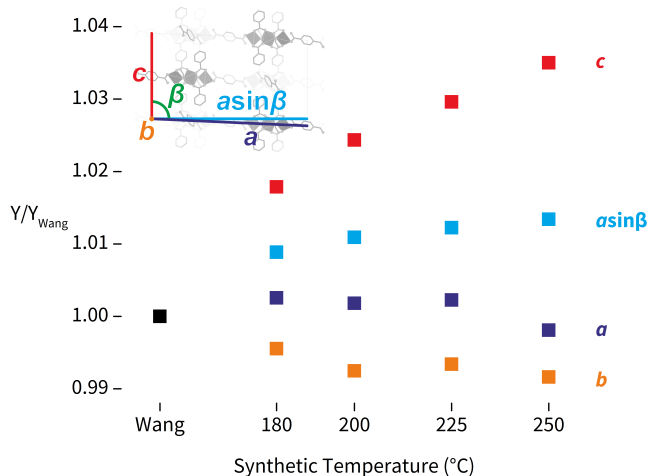


Figure 3. Change in cell parameters of Co-BDC-DMF reaction products synthesised at different temperatures

Previous work has shown that by either layer shearing and/or variable coordination of the cobalt cluster, a range of possible cell parameters are possible within the  $C2/c$  space group. Our study demonstrates a systematic variation in cell parameters depending on synthesis temperature (Figure 3). Due to the low symmetry and large asymmetric unit of this structure, structures could not be unambiguously determined from Rietveld refinement. However, comparative refinement with different structural models suggests that at a synthetic temperature of 250 °C, the structure tends toward a framework containing  $\text{Co}_{\text{tet}}\text{-Co}_{\text{oct}}\text{-Co}_{\text{tet}}$  clusters (comparative refinements included in ESI). At lower synthetic temperatures, refinement does not easily differentiate, but cell parameters are closer to known frameworks with the  $\text{Co}_{\text{oct}}\text{-Co}_{\text{oct}}\text{-Co}_{\text{oct}}$  coordination.

## Conclusions

Time-resolved *in situ* ADXRD using high energy X-ray radiation has allowed us to probe the mechanism and kinetics of the hydrothermal synthesis of  $(\text{H}_2\text{NMe}_2)_2[\text{Co}_3(\text{BDC})_4]\cdot y\text{DMF}$ . The crystallization of  $(\text{H}_2\text{NMe}_2)_2[\text{Co}_3(\text{BDC})_4]\cdot y\text{DMF}$  proceeds *via* a structurally-related metastable precursor, in which layer structure is preserved while the inter-layer ordering changes. The observation of a Bragg reflection that remains throughout the transition indicates that the process is topotactic rearrangement.

## Experimental Section

**General procedures for resin-assisted synthesis.** Sulfonated styrene-divinylbenzene (styrene-DVB) beads were purchased in the  $\text{Na}^+$  form (DOWEX® MARATHON® C) from Sigma-Aldrich. The beads were converted to the  $\text{Co}^{2+}$  metal-exchanged form by treatment with  $\text{CoCl}_2$ . 6 g of styrene-DVB beads were added to 30 mL of a saturated aqueous solution of  $\text{CoCl}_2$  and stirred for 3 hours at room temperature. The mixture was vacuum filtered to isolate the beads, and the resulting cobalt-exchanged beads were

washed with deionised water and dried in air. This procedure was repeated a further four times to ensure significant metal ion exchange. The beads were then used in place of typical metal salt precursors.

**Angular-dispersive *in situ* XRD.** Angular-dispersive XRD was employed to monitor the resin-assisted solvothermal synthesis of frameworks in the Co-NDC-DMF system. Reactions were undertaken at Beamline I12, Diamond Light Source, using the Oxford-Diamond *In Situ* Cell (ODISC) furnace in the hydrothermal configuration.<sup>13</sup> Data were collected using a Thales Pixium image plate detector (430 x 430 mm<sup>2</sup>), with 4 s exposures collected at 30 s intervals. The system was calibrated with a crystalline CeO<sub>2</sub> reference and the 2D image plate data were integrated using the fit2d software to give 1D diffraction patterns.<sup>19</sup> The energy of the monochromated beam was 53.2442 keV ( $\lambda = 0.23286 \text{ \AA}$ ) and the detector was positioned 2501.440 mm from the sample. An X-ray beam size of 0.5 x 0.5 mm was used.

0.4 g 1,4-BDC were dissolved in 12 ml DMF. 4 mL methanol and 0.5 g cobalt-exchanged resin beads were added to the solution and the mixture placed in a PTFE liner and sealed inside a stainless-steel autoclave. Autoclaves containing the reaction mixture were heated at 30 °C min<sup>-1</sup> to the dwell temperature (180, 200, 225, or 250 °C) and held until the reaction was deemed to have reached completion. Following cooling, the sample was transferred to a polypropylene centrifuge tube and a 4 s scan of the product was collected. Refinements on powder XRD data were performed using GSAS through the EXPGUI interface.<sup>20,21</sup>

[Background subtraction details]

## ASSOCIATED CONTENT

### Supporting Information. ....

This material is available free of charge via the Internet at <http://pubs.acs.org>.

## AUTHOR INFORMATION

### Corresponding Author

\*E-mail: [dermot.ohare@chem.ox.ac.uk](mailto:dermot.ohare@chem.ox.ac.uk)

### Author Contributions

‡These authors contributed equally.

### Notes

The authors declare no competing financial interest.

## ACKNOWLEDGMENT

The authors would like to acknowledge: Engineering and Physical Sciences Research Council (U.K.) (EPSRC) and the Diamond Light Source Ltd. for provision of a research studentship (S.J.M.); this work is funded by the European Union's Seventh Framework Programme (FP7/2007–2013), grant agreement no. FP7-NMP4-LA-2012-280983, SHYMAN; Dr Andrew Jupe for assistance with data manipulation; Michael Drakopoulos and all the staff of Beamline I12 at the Diamond

Light Source for assistance with *in situ* diffraction experiments.

## REFERENCES

- (1) El Osta, R.; Feyand, M.; Stock, N.; Millange, F.; Walton, R. I. *Powder Diffr.* **2013**, 28 (SupplementS2), S256.
- (2) Millange, F.; Medina, M. I.; Guillou, N.; Férey, G.; Golden, K. M.; Walton, R. I. *Angew. Chemie Int. Ed.* **2010**, 49 (4), 763.
- (3) Millange, F.; El Osta, R.; Medina, M. E.; Walton, R. I. *CrystEngComm* **2011**, 13 (1), 103.
- (4) Cravillon, J.; Schroder, C. A.; Bux, H.; Rothkirch, A.; Caro, J.; Wiebcke, M. *CrystEngComm* **2012**, 14 (2), 492.
- (5) Ragon, F.; Horcajada, P.; Chevreau, H.; Hwang, Y. K.; Lee, U. H.; Miller, S. R.; Devic, T.; Chang, J. S.; Serre, C. *Inorg. Chem.* **2014**, 53 (5), 2491.
- (6) Ragon, F.; Campo, B.; Yang, Q.; Martineau, C.; Wiersum, A. D.; Lago, A.; Guillerm, V.; Hemsley, C.; Eubank, J. F.; Vishnuvarthan, M.; Taulelle, F.; Horcajada, P.; Vimont, A.; Llewellyn, P. L.; Daturi, M.; Devautour-Vinot, S.; Maurin, G.; Serre, C.; Devic, T.; Clet, G. *J. Mater. Chem. A* **2015**, 3 (7), 3294.
- (7) Ragon, F.; Chevreau, H.; Devic, T.; Serre, C.; Horcajada, P. *Chem. - A Eur. J.* **2015**, 21 (19), 7135.
- (8) Zahn, G.; Zerner, P.; Lippke, J.; Kempf, F. L.; Lilienthal, S.; Schröder, C. A.; Schneider, A. M.; Behrens, P. *CrystEngComm* **2014**, 16 (39), 9198.
- (9) Friščić, T.; Halasz, I.; Beldon, P. J.; Belenguer, A. M.; Adams, F.; Kimber, S. A. J.; Honkimäki, V.; Dinnebier, R. E. *Nat. Chem.* **2013**, 5 (1), 66.
- (10) Stavitski, E.; Goesten, M.; Juan-Alcañiz, J.; Martinez-Joaristi, A.; Serra-Crespo, P.; Petukhov, A. V.; Gascon, J.; Kapteijn, F. *Angew. Chemie Int. Ed.* **2011**, 50 (41), 9624.
- (11) Goesten, M.; Stavitski, E.; Pidko, E. A.; Gücüyener, C.; Boshuizen, B.; Ehrlich, S. N.; Hensen, E. J. M.; Kapteijn, F.; Gascon, J. *Chem. - A Eur. J.* **2013**, 19 (24), 7809.
- (12) Patterson, J. P.; Abellan, P.; Denny, M. S.; Park, C.; Browning, N. D.; Cohen, S. M.; Evans, J. E.; Gianneschi, N. C. *J. Am. Chem. Soc.* **2015**, 137 (23), 150608120034003.
- (13) Moorhouse, S. J.; Vranješ, N.; Jupe, A.; Drakopoulos, M.; O'Hare, D.; Vranje, N.; Jupe, A.; Drakopoulos, M.; O'Hare, D. *Rev. Sci. Instrum.* **2012**, 83 (8), 084101.
- (14) Du, Y.; Hu, G.; O'Hare, D. *J. Mater. Chem.* **2009**, 19 (8), 1160.
- (15) Du, Y.; Thompson, A. L.; O'Hare, D. *Chem. Commun.* **2008**, No. 45, 5987.

- (16) Du, Y.; Thompson, A. L.; Russell, N.; O'Hare, D. *Dalt. Trans.* **2010**, 39 (14), 3384.
- (17) Kondo, M.; Takashima, Y.; Seo, J.; Kitagawa, S.; Furukawa, S. *CrystEngComm* **2010**, 12 (8).
- (18) Wang, X.-F.; Zhang, Y.-B.; Xue, W.; Qi, X.-L.; Chen, X.-M. *CrystEngComm* **2010**, 12 (11), 3834.
- (19) Hammersley, A. P.; Svensson, S. O.; Hanfland, M.; Fitch, A. N.; Hausermann, D. *High Press. Res.* **1996**, 14 (4-6), 235.
- (20) Toby, B. H. *J. Appl. Crystallogr.* **2001**, 34 (2), 210.
- (21) Von Dreele, R.; Larson, A. *General structure analysis system (GSAS)*; 1994.

To format double-column figures, schemes, charts, and tables, use the following instructions:

Place the insertion point where you want to change the number of columns

From the **Insert** menu, choose **Break**

Under **Sections**, choose **Continuous**

Make sure the insertion point is in the new section. From the **Format** menu, choose **Columns**

In the **Number of Columns** box, type **1**

Choose the **OK** button

Now your page is set up so that figures, schemes, charts, and tables can span two columns. These must appear at the top of the page. Be sure to add another section break after the table and change it back to two columns with a spacing of 0.33 in.

**Table 1. Example of a Double-Column Table**

Column 1	Column 2	Column 3	Column 4	Column 5	Column 6	Column 7	Column 8

Authors are required to submit a graphic entry for the Table of Contents (TOC) that, in conjunction with the manuscript title, should give the reader a representative idea of one of the following: A key structure, reaction, equation, concept, or theorem, etc., that is discussed in the manuscript. Consult the journal's Instructions for Authors for TOC graphic specifications.

---

Insert Table of Contents artwork here

---